J|A|C|S
ARTICLES
Published on Web 05/16/2007

Shape-Controlled Conversion of β-Sn Nanocrystals into Intermetallic *M*-Sn (*M* = Fe, Co, Ni, Pd) Nanocrystals

Nam Hawn Chou and Raymond E. Schaak*

Contribution from the Department of Chemistry, Texas A&M University, College Station, Texas 77842-3012

Received December 17, 2006; E-mail: schaak@mail.chem.tamu.edu

Abstract: The ability to control the shape of metal nanocrystals is critical to applications such as catalysis, magnetism, and plasmonics. Despite significant advances in controlling the shapes of single-metal nanocrystals, rigorous shape control of multimetal nanocrystals remains challenging, and has been limited largely to alloy systems of similar metals. Here we describe a robust strategy that produces shape-controlled intermetallic nanocrystals involving elements of notably different reduction potentials, reduction kinetics, and reactivity. The approach utilizes shape- and size-controlled β-Sn nanocrystals as reactive templates that can be converted into binary *M*-Sn (*M* = Fe, Co, Ni, Pd) intermetallic compounds by reaction with appropriate metal salt solutions under reducing conditions. The result, demonstrated in detail for the $FeSn_2$ system, is a variety of nanostructures with morphologies that include spheres, cubes, hollow squares, U-shaped structures, nanorods, and nanorod dimers. Our experiments demonstrate a size- and shape-dependent reactivity toward the formation of hollow $FeSn_2$ nanostructures and provide empirical guidelines for the formation of other intermetallic nanocrystals. In addition to those of $FeSn_2$, nanocrystals of intermetallic PdSn, $CoSn_3$, and $NiSn_3$ can be formed using this same chemical conversion strategy.

Introduction

Template-based strategies are becoming increasingly common for synthesizing nanoscale inorganic solids with complex morphologies. For example, *nonreactive* templates, such as colloidal crystals[1] and porous alumina membranes,[2] can serve as physical molds for the deposition of many types of materials. Likewise, metal nanoparticles can serve as *reactive* templates that help to define the shape and composition of derivative nanostructures after carrying out appropriate chemical transformations.[3] Some of the many recent examples of the latter include hollow Au nanoboxes formed by templating against Ag nanocubes,[4] Ag_2Se nanowires formed by reacting Se nanowires with a solution of $AgNO_3$,[5] hollow cobalt sulfide nanospheres formed by reacting Co nanoparticles with sulfur,[6] and hollow CoPt alloy nanospheres formed from the reaction of Co nanoparticles with aqueous K_2PtCl_6 under reducing conditions.[7] The strategies that utilize metal nanoparticle templates generally succeed at producing shape-controlled nanostructures with morphologies that can be difficult or impossible to prepare using other synthetic methods, including 1D nanowires, cube-shaped nanocrystals, and hollow nanostructures.

The ability to control the shape of metal nanocrystals is important because it is central to applications such as catalysis and plasmonics.[8] For example, cubes and tetrahedra expose different crystal facets, and each shows unique catalytic capabilities that may be exploited to fine-tune catalytic activity and selectivity.[9] Likewise, dense spheres, hollow spheres, cubes, rods, and triangles each have unique plasmonic properties that can be fine-tuned by changing their shape.[10] Despite significant advances in controlling the shape of metal nanocrystals,[11] particularly through template-based strategies, rigorous shape control of multimetal nanocrystals remains challenging. To date, there have been no examples of rigorous shape control in multimetal intermetallic systems with elements of notably different reduction potentials, reduction kinetics, and reactivity.

Here we show that β-Sn nanocrystals can serve as templates for the formation of shape-controlled intermetallic nanocrystals using solution-mediated reactions with transition metal salts. In addition to accessing nanocrystal morphologies that have not

(1) (a) Stein, A.; Schroden, R. C. *Curr. Opin. Solid State Mater. Sci.* **2001**, *5*, 553−564. (b) Jiang, P.; Bertone, J. F.; Colvin, V. L. *Science* **2001**, *291*, 453−457.
(2) Kline, T. R.; Tian, M.; Wang, J.; Sen, A.; Chan, M. W. H.; Mallouk, T. E. *Inorg. Chem.* **2006**, *45*, 7555−7565.
(3) Wiley, B.; Sun, Y. G.; Mayers, B.; Xia, Y. N. *Chem. Eur. J.* **2005**, *11*, 454−463.
(4) Sun, Y. G.; Xia, Y. N. *Science* **2002**, *298*, 2176−2179.
(5) (a) Gates, B.; Wu, Y.; Yin, Y.; Yang, P.; Xia, Y. *J. Am. Chem. Soc.* **2001**, *123*, 11500−11501. (b) Gates, B.; Mayers, B.; Wu, Y.; Sun, Y.; Cattle, B.; Yang, P.; Xia, Y. *Adv. Funct. Mater.* **2002**, *12*, 679−868. (c) Jeong, U.; Camargo, P. H. C.; Lee, Y. H.; Xia, Y. *J. Mater. Chem.* **2006**, *16*, 3893−3897.
(6) Yin, Y.; Rioux, R. M.; Erdonmez, C. K.; Hughes, S.; Somorjai, G. A.; Alivisatos, A. P. *Science* **2004**, *304*, 711−714.
(7) Vasquez, Y.; Sra, A. K.; Schaak, R. E. *J. Am. Chem. Soc.* **2005**, *127*, 12504−12505.
(8) (a) Burda, C.; Chen, X.; Narayanan, R.; El-Sayed, M. A. *Chem. Rev.* **2005**, *105*, 1025−1102. (b) Eustis, S.; El-Sayed, M. A. *Chem. Soc. Rev.* **2006**, *35*, 209−217.
(9) (a) Narayanan, R.; El-Sayed, M. A. *J. Am. Chem. Soc.* **2004**, *126*, 7194−7195. (b) Narayanan, R.; El-Sayed, M. A. *Nano Lett.* **2004**, *4*, 1343−1348.
(10) (a) Murphy, C. J.; Jana, N. R. *Adv. Mater.* **2002**, *14*, 80−82. (b) Guo, L.; Murphy, C. J. *Chem. Mater.* **2005**, *17*, 3668−3672. (c) Xiong, Y.; McLellan, J. M.; Chen, J.; Yin, Y.; Li, Z.-Y.; Xia, Y. *J. Am. Chem. Soc.* **2005**, *127*, 17118−17127. (d) Liang, H.-P.; Wan, L.-J.; Bai, C.-L.; Jiang, L. *J. Phys. Chem. B* **2005**, *109*, 7795−7800. (e) Wang, H.; Tam, F.; Grady, N. K.; Halas, N. J. *J. Phys. Chem. B* **2005**, *109*, 18218−18222. (f) Wang, H.; Brandl, D. W.; Le, F.; Nordlander, P.; Halas, N. J. *Nano Lett.* **2006**, *6*, 827−832.

yet been achieved for multimetal intermetallic systems, this template-based strategy also appears to yield crystal structures that can be difficult to access by traditional solid-state synthetic methods. To demonstrate this approach and to generate guidelines for the formation of shape-controlled intermetallic nanocrystals, we focus initially on $FeSn_2$, which is an antiferromagnet that is sometimes used as a component in exchange-biased films.[12] We then extend the strategy to intermetallic PdSn, which is a known catalyst.[13] Finally, we show that the same approach also generates nanocrystals of $CoSn_3$ and $NiSn_3$. $CoSn_3$ is a low-temperature intermetallic phase that was only recently discovered,[14] and it can be difficult to synthesize using traditional high-temperature solid-state methods. $NiSn_3$ does not appear on the Ni−Sn phase diagram.[15]

Experimental Section

Chemicals. All chemicals were purchased from Alfa Aesar and were used as received without further processing or purification: $FeCl_3 \cdot 6H_2O$ (97.0−102.0%), $SnCl_2$ (anhydrous, 99% min.), $CoCl_2 \cdot 6H_2O$ (98.0−102.0%), $NiCl_2 \cdot 6H_2O$ (99.95%), and $Pd(acac)_2$ (Pd 34.63%). The reducing agent, surface stabilizer, and solvent were $NaBH_4$ (98%), poly(vinyl pyrrolidone) (PVP, MW = 40 000, 630 000, or 1 300 000), and tetraethylene glycol (TEG, 99+%), respectively. 1,2-Dichlorobenzene (98+%) was also used in some cases, as described below.

Synthesis of Intermetallic Nanostructures. Intermetallic *M*-Sn (*M* = Fe, Co, Ni, Pd) nanocrystals were synthesized by sequential $NaBH_4$ reduction of the metal salts in tetraethylene glycol (TEG), followed by heating to 170−205 °C under Ar in the presence of PVP (MW = 40 000) and/or other polymers such as poly(2-ethyl-2-oxazoline) (PEO; MW = 50 000). In a typical synthesis of $FeSn_2$ nanocrystals, 0.7 g of PVP and 0.3 g of PEO were dissolved in 45 mL of TEG at room temperature. The solution was heated to 170 °C, and then $SnCl_2$ (0.130 g in 4 mL of TEG) was added. A freshly prepared solution of $NaBH_4$ (0.264 g in 8 mL of TEG) was then added dropwise while stirring. After 12−15 min at 170 °C, $FeCl_3 \cdot 6H_2O$ (0.090 g in 4 mL of TEG) was added. The resulting solution was heated to 170−205 °C for 1−2 h, resulting in a black colloidal solution. The $FeSn_2$ nanocrystals were isolated by centrifugation and washed with ethanol.

The same approach was used for PdSn, except that $SnCl_2$ (0.13 g in 4 mL of TEG) and $Pd(acac)_2$ (0.10 g in 4 mL of 1,2-dichlorobenzene) were used, and the final solution was heated to 170−190 °C for 30 min before isolating the black colloidal PdSn solution. For $CoSn_3$, $SnCl_2$ (0.13 g in 4 mL of TEG) and $CoCl_2 \cdot 6H_2O$ (0.05 g in 4 mL of TEG) were used, and the final solution was heated to 180−195 °C for 1.5 h, resulting in a black colloidal $CoSn_3$ solution. For $NiSn_3$, $SnCl_2$ (0.13 g in 4 mL of TEG) and $NiCl_2 \cdot 6H_2O$ (0.05 g in 4 mL of TEG) were used, and the final solution was heated to 150 °C for 1.5 h.

Synthesis of β-Sn Nanocrystal Shapes. Unless otherwise noted, 0.7 g of PVP (MW = 40 000) and 0.3 g of PEO (MW = 50 000) were dissolved in 45 mL of TEG at room temperature. The solution was heated to various temperatures (described below), and then $SnCl_2$ (0.13 g in 4 mL of TEG) was added. A freshly prepared solution of $NaBH_4$ (0.264 g in 8 mL of TEG) was then added dropwise while stirring. After 12−15 min, the resulting solution was removed from the heat, and the black-colored β-Sn nanocrystals were isolated by centrifugation and washed with ethanol. For the synthesis of predominantly large (>30 nm) cube-shaped β-Sn nanocrystals, the temperature was 170 °C. To generate a mixture of large (>30 nm) and small (<15 nm) cube-shaped β-Sn nanocrystals, the temperature was 140 °C. To generate predominantly large (>20 nm) spherical β-Sn nanocrystals, PVP with a molecular weight of 630 000 was used, and the temperature was 170 °C. For smaller (<10 nm) β-Sn nanocrystal spheres, 0.4 g of PVP (MW = 630 000) was used without any PEO present, $SnCl_2$ was added at 80 °C, and the final solution temperature was 140 °C.

To access β-Sn nanorods, 0.4 g of PVP (MW = 630 000) was dissolved in 45 mL of TEG at room temperature. $SnCl_2$ (0.08 g in 4 mL of TEG) was then added, along with a freshly prepared solution of $NaBH_4$ (0.264 g in 8 mL of TEG) while stirring. The temperature was gradually increased to 120 °C over 40 min. Concurrently, β-Sn seed nanocrystals were prepared by sequentially adding 0.15 g of PVP, 0.025 g of $SnCl_2$, and 0.13 g of $NaBH_4$ to 8 mL of TEG. This solution of β-Sn seed nanocrystals was added to the original β-Sn nanocrystal solution at 120 °C before increasing the temperature to 160 °C for 1 h, and then another solution of β-Sn seed nanocrystals was added. The temperature was increased to 190 °C, and then the solution was removed from the heat. The predominantly rod-shaped β-Sn nanocrystals were isolated by centrifugation and washed with ethanol.

Characterization. Powder X-ray diffraction (XRD) data were collected on either a Bruker GADDS three-circle X-ray diffractometer using Cu Kα radiation or on a Bruker D-8 Advance powder diffractometer. Transmission electron microscopy (TEM) images, selected area electron diffraction (SAED) patterns, and energy dispersive X-ray spectroscopy (EDS) were collected using a JEOL JEM-2010 TEM. Samples for TEM analysis were prepared by dropping an ethanol solution containing the β-Sn or *M*-Sn nanoparticles onto the surface of a carbon-coated copper or nickel grid. Elemental analysis was performed using a Perkin-Elmer DRCII inductively coupled plasma mass spectrometer (ICP-MS).

Results and Discussion

Generation of Hollow Cube-Derived $FeSn_2$ Nanostructures. TEM images of representative $FeSn_2$ nanocrystals are shown in Figures 1 and 2. SAED (Figure 1a), XRD (Figure 1b), and EDS (Figure S1) data confirm that the composition and structure match that of $CuAl_2$-type $FeSn_2$. Interestingly, the nanocrystals adopt a variety of shapes that consist predominantly of hollow squares, U-shaped structures, and nanorods that are typically associated as dimers (Figure 2). Most of the $FeSn_2$ shapes consist of single-domain crystals (Figure 1c). Because the nanocrystals are predominantly cube-shaped and roughly uniform in size (although not rigorously monodisperse), they have a tendency to align into one-dimensional superstructures (Figure 2a−e). The $FeSn_2$ nanocrystals are each generally capped with a 1−2 nm SnO_x shell, as determined by TEM and XPS.

A closer look at the reaction provides important insights into how the intermetallic $FeSn_2$ nanocrystal shapes are formed and how their shape and size can be influenced by adjusting the

(11) (a) Puntes, V. F.; Krishnan, K. M.; Alivisatos, A. P. *Science* **2001**, *291*, 2115−2117. (b) Jin, R.; Cao, Y.; Mirkin, C. A.; Kelly, K. L.; Schatz, G. C.; Zheng, J. G. *Science* **2001**, *294*, 1901−1903. (c) Sun, Y.; Xia, Y. *Science* **2002**, *298*, 2176−2179. (d) Chen, S.; Wang, Z. L.; Ballato, J.; Foulger, S. H.; Carroll, D. L. *J. Am. Chem. Soc.* **2003**, *125*, 16186−16187. (e) Dumestre, F.; Chaudret, B.; Amiens, C.; Respaud, M.; Fejes, P.; Renaud, P.; Zurcher, P. *Angew. Chem., Int. Ed.* **2003**, *42*, 5213−5216. (f) Sau, T. K.; Murphy, C. J. *J. Am. Chem. Soc.* **2004**, *126*, 8648−8649. (g) Dumestre, F.; Chaudret, B.; Amiens, C.; Renaud, P.; Fejes, P. *Science* **2004**, *303*, 821−823. (h) Kim, F.; Connor, S.; Song, H.; Kuykendall, T.; Yang, P. *Angew. Chem., Int. Ed.* **2004**, *43*, 3673−3677. (i) Teng, X.; Yang, H. *Nano Lett.* **2005**, *5*, 885−891. (j) Song, H.; Kim, F.; Connor, S.; Somorjai, G. A.; Yang, P. *J. Phys. Chem. B* **2005**, *109*, 188−193. (k) Hoefelmeyer, J. D.; Niesz, K.; Somorjai, G. A.; Tilley, T. D. *Nano Lett.* **2005**, *5*, 435−438.

(12) (a) Venturini, G.; Malaman, B.; Le Caer, G.; Fruchart, D. *Phys. Rev. B* **1987**, *35*, 7038−7045. (b) Stromberg, F.; Keune, W.; Kuncser, V. E.; Westerholt, K. *Phys. Rev. B* **2005**, *72*, 064440.

(13) (a) Bodnariuk, P.; Coq, B.; Ferrat, G.; Figueras, F. *J. Catal.* **1989**, *116*, 459−466. (b) Sales, E. A.; Mendes, M. J.; Bozon-Verduraz, F. *J. Catal.* **2000**, *195*, 96−105.

(14) (a) Lang, A.; Jeitschko, W. *Z. Metallkunde* **1996**, *87*, 759−764. (b) Kanatzidis, M. G.; Pöttgen, R.; Jeitschko, W. *Angew. Chem., Int. Ed.* **2005**, *44*, 6996−7023.

(15) (a) Massalski, T. B., Ed. *Binary Alloy Phase Diagrams*; ASM International: Materials Park, OH, 1996. (b) Kim, S.; Johnson, D. C. *J. Alloys Compd.* **2005**, *392*, 105−111.

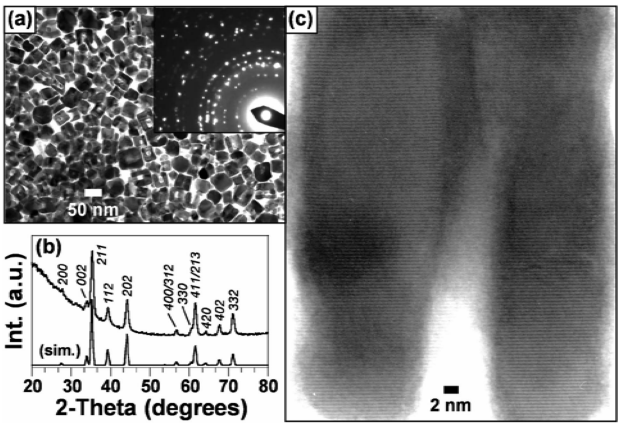

Figure 1. (a) TEM micrograph and SAED pattern (inset) of $FeSn_2$ nanocrystal shapes; (b) powder XRD pattern (top: experimental; bottom: simulated); (c) HRTEM image of a single-domain $FeSn_2$ nanocrystal.

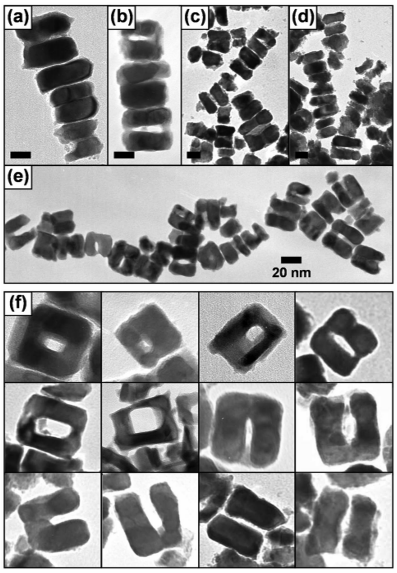

Figure 2. TEM micrographs of (a−e) assemblies of cube-derived $FeSn_2$ nanocrystals and (f) representative nanocrystal shapes (each ∼50 nm), including hollow squares, U-shaped structures, and nanorod dimers. Scale bars in (a−d) are 15 nm.

reaction conditions. During the reaction, Sn nanocrystals are formed first by $NaBH_4$ reduction of Sn^{2+}; then Fe^{3+} is added to the Sn nanocrystals under reducing conditions (excess $NaBH_4$) to form $FeSn_2$. A representative TEM image of the Sn nanoparticle seeds is shown in Figure 3a; SAED (Figure 3a, inset) and XRD (Figure S2) data confirm the formation of β-Sn. Careful control over the synthetic conditions can lead to predominantly (∼90%) single-domain cube-shaped nanocrystals (Figure 3a) of β-Sn, although some spherical particles are usually observed.

These cube-shaped β-Sn nanocrystals serve as reactive templates for chemical transformation into $FeSn_2$ with retention of the cubic morphology. Importantly, the β-Sn nanocrystals can be isolated, redispersed in TEG without any excess Sn salts, and then reacted with Fe^{3+} under reducing conditions ($NaBH_4$) to form $FeSn_2$. This confirms that the β-Sn nanocrystals serve as seeds for transformation into $FeSn_2$. Chemical analysis (ICP) of the $FeSn_2$ solution after removing the $FeSn_2$ nanocrystals by centrifugation confirms that only trace amounts of Sn are present in the supernatant, which indicates that all of the Sn in the β-Sn

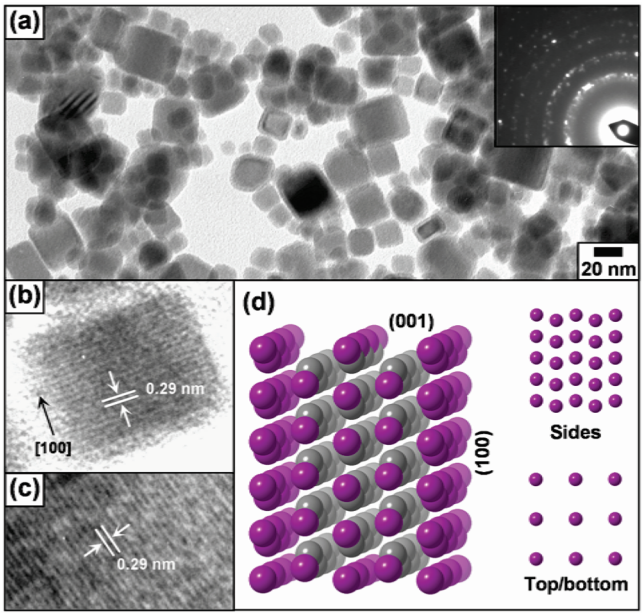

Figure 3. (a−c) TEM micrographs for Sn nanocrystal seeds (SAED pattern shown in the inset) and (d) crystal structure of β-Sn (purple represents surface atoms; gray represents interior atoms), showing the atom density on the side and top/bottom surfaces.

nanocrystal seeds is incorporated into the $FeSn_2$ product. Thus, the reaction is not likely to be a galvanic replacement reaction, which would eject Sn^{2+} back into the supernatant as predicted by the reaction necessary to generate $FeSn_2$ by this route:

$$7\ Sn^0 + 2\ Fe^{3+} \rightarrow 2\ FeSn_2 + 3\ Sn^{2+}$$

Rather, it is more likely to be a diffusion-based process where Fe diffuses into Sn. This assignment is also supported by the fact that $CoSn_2$ and Ni_3Sn_4 can be generated using the same route (Figure S2): β-Sn nanocrystals are synthesized by $NaBH_4$ reduction of Sn^{2+} in TEG, then isolated, redispersed in fresh TEG with no $NaBH_4$, and reacted with Co^{2+} to form $CoSn_2$ after heating to ∼200 °C. Ni_3Sn_4 can be formed similarly by reacting Sn nanocrystals with Ni^{2+} in TEG with no $NaBH_4$ present. While $FeSn_2$ could in principle be formed via a galvanic displacement reaction between Sn nanoparticles and Fe^{3+} based on the reduction potentials of the Fe^{3+}/Fe^0 (−0.037 eV) and Sn^{2+}/Sn^0 (−0.1375 eV) redox couples, $CoSn_2$ and Ni_3Sn_4 could not, since the reduction potentials of the Co^{2+}/Co^0 (−0.28 eV) and Ni^{2+}/Ni^0 (−0.257 eV) couples are more negative than that of Sn^{2+}/Sn^0.

The shape-conserving reactivity and the formation of hollowed-out nanostructures can be rationalized by considering the crystal structure, morphology, and diffusion characteristics of the β-Sn nanoparticle templates (Figure 3d). The lattice fringes of the single-crystal β-Sn nanocubes (Figure 3b,c) indicate that the ⟨100⟩ crystallographic faces are exposed, consistent with previous reports of β-Sn nanowires.[16] The structure of β-Sn is highly anisotropic: the top and bottom faces have a low density of surface atoms, while the four side faces have a much higher atomic density (Figure 3d). β-Sn is known to have different diffusion rates along the *a*- and *c*-axes as well, with the rate of diffusion along each axis being dependent upon the metal that

(16) (a) Hsu, Y.-J.; Lu, S.-Y. *J. Phys. Chem. B* **2005**, *109*, 4398−4403. (b) Hsu, Y.-J.; Lu, S.-Y.; Lin, Y.-F. *Small* **2006**, *2*, 268−273.

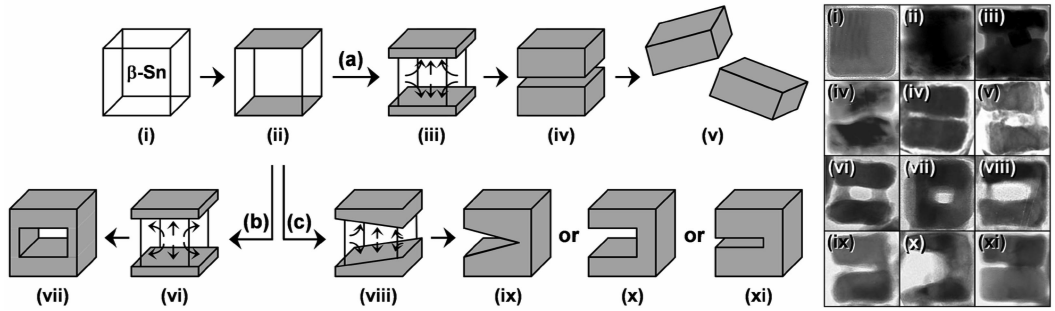

Figure 4. Schematic outlining a hypothesized pathway for the formation of the observed $FeSn_2$ cube-derived nanostructures via an anisotropic Kirkendall-type mechanism. All structures can be derived from preferential Fe absorption on the top and bottom *100* faces of β-Sn nanocrystal cubes, with subsequent anisotropic diffusion into the structure. In (a), uniform outward diffusion from the center of the cube produces slabs (nanorods or nanoplates) which, if not held together by residual surface oxide or by $FeSn_2$ bridges, can dissociate to form free-standing particles. (They often remain associated as dimers, which follows directly from this proposed hollowing process.) In (b), diffusion initially occurs fastest from the center, hollowing out from the center to form square-shaped structures. In (c), the diffusion and hollowing process is not uniform, proceeding in one direction faster than the other (possibly caused by subtle kinetic or steric effects), resulting in partially hollow (U-shaped) structures. Several morphologies are possible, depending on subtle and as-yet uncontrollable details about how the reaction proceeds. TEM micrographs of aliquots taken during reactions show examples of reaction intermediates that are consistent with the proposed formation pathway. Selected examples are shown to the right and labeled according to the schematic drawing that they most closely match.

is diffusing into the β-Sn crystal.[17] Furthermore, because of the higher atomic density of Sn atoms on the four side faces relative to the top and bottom faces (Figure 3d), the top and bottom faces are likely to be more reactive in solution than the sides, with the polymer being better able to adsorb to and stabilize the side faces, helping to inhibit their reactivity.

On the basis of all of these considerations, it is surmised that Fe absorption and diffusion into β-Sn is more likely to occur via the top and bottom faces. Consistent with this, the β-Sn cubes tend to transform into hollow cube-derived nanostructures (Figure 1 and 2), hollowing out from the center. The schematic shown in Figure 4 rationalizes the formation of each of the observed shapes based on this reaction pathway, which considers both preferential stabilization of the four side faces and the known anisotropic diffusion characteristics of β-Sn. In a few cases, reaction intermediates can be isolated and observed by TEM (Figure 4), providing some support for the proposed formation pathway. We can roughly control the degree of reactivity to create predominantly hollow structures vs nanorods. However, we are unable at this point to control, to a large extent, which morphologies are favored during the reaction. This implies that it is dependent on subtle reaction conditions and possibly on variations in the size and shape of the Sn precursors, for which there are no reports of highly monodisperse shape-controlled nanocrystals in the literature. Consistent with this, all morphologies are accessible in statistically similar yields. Additional work to identify the reaction conditions necessary to preferentially access each of the morphologies is in progress.

This reactivity provides further evidence of the mechanism that is likely to be responsible for the formation of hollow cube-derived $FeSn_2$ nanostructures. Chemical analysis, discussed earlier, argues against galvanic replacement, since Sn is not removed during the deposition of Fe. Also, standard reduction potentials are inconsistent with a galvanic replacement mechanism, since control experiments (discussed earlier) confirm that $CoSn_2$ and Ni_3Sn_4 can form under conditions identical to those used for $FeSn_2$. Furthermore, excess Sn would be required for $FeSn_2$ to form via a galvanic replacement reaction, since some Sn would have to be sacrificially oxidized as Fe^{3+} reduces. The fact that Fe and Sn are present in a stoichiometric (1:2) ratio both before the reaction and in the final product also argues against a galvanic replacement mechanism, since such a reaction would yield a product composition that differs from the nominal reaction stoichiometry. Another possible mechanism involves the formation of oxide particles or an oxide layer, e.g., SnO_2 or Fe_2O_3, during the reaction. All of the Sn nanocrystals and many of the $FeSn_2$ nanocrystals are capped with a 1−2 nm SnO_x shell, as determined by TEM and XPS. However, it is likely that the oxide coating forms as a result of oxidation of the Sn metal nanocrystals rather than as a result of a reaction between the transition metal and Sn. Similar SnO_x shells have been observed on many Sn-containing nanocrystals synthesized using related polyol-based techniques that do not rigorously exclude air,[18,19] and the oxide shells tend to remain inert despite subsequent chemistry that modifies the compositions and structures of the metal cores.[19]

Thus, considering all of the available data that argue against galvanic displacement, the mechanism is most likely to be a Kirkendall process, where Fe metal deposits onto the Sn nanoparticles and the different diffusion rates of the different species in an anisotropic manner cause a depletion of material in the center of the nanostructure.[6] This is also consistent with the known diffusion characteristics of Sn and Fe, where Sn would be expected to diffuse faster than Fe.[17] Kirkendall effects have previously been implicated in the synthesis of hollow spherical structures,[6,20−21] but not the complex cube-derived structures shown here. Our results with the $FeSn_2$ system imply that anisotropic Kirkendall effects can lead to quite elaborate nanostructures with a range of shapes.

Size- and Shape-Dependent Reactivity. Since the chemical transformation of β-Sn into $FeSn_2$ conserves the cubic shape

(17) (a) Seitz, F.; Turnbull, D.; Ehrenreich, H. *Solid State Physics*; Academic Press: New York, 1968; Vol. 22. (b) Van Beek, J. A.; Stolk, S. A.; Van Loo, F. J. *Z. Metallkunde* **1982**, *73*, 439−444.

(18) Cable, R. E.; Schaak, R. E. *Chem. Mater.* **2005**, *17*, 6835−6841.

(19) (a) Leonard, B. M.; Bhuvanesh, N. S. P.; Schaak, R. E. *J. Am. Chem. Soc.* **2005**, *127*, 7326−7327. (b) Leonard, B. M.; Schaak, R. E. *J. Am. Chem. Soc.* **2006**, 11475−11482.

(20) (a) Liu, B.; Zeng, H. C. *J. Am. Chem. Soc.* **2004**, *126*, 16744−16746. (b) Fan, H. J.; Knez, M.; Scholz, R.; Nielsch, K.; Pippel, E.; Hesse, D.; Zacharias, M.; Gösele, U. *Nat. Mater.* **2006**, *5*, 627−631.

(21) (a) Henkes, A. E.; Vasquez, Y.; Schaak, R. E. *J. Am. Chem. Soc.* **2007**, *129*, 1896−1897. (b) Chiang, R.-K.; Chiang, R.-T. *Inorg. Chem.* **2007**, *46*, 369−371.

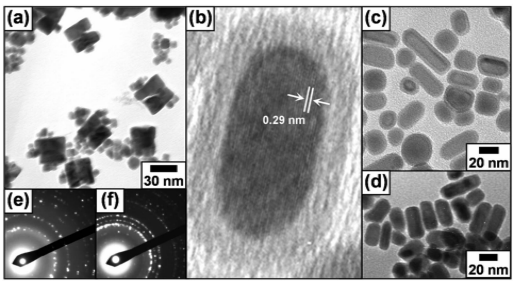

Figure 5. (a) TEM micrograph of bimodal $FeSn_2$ nanocrystals (>30 nm and <15 nm) synthesized by reacting similarly bimodal β-Sn nanocrystals with Fe^{3+} under reducing conditions. The larger (>30 nm) $FeSn_2$ nanocubes are partially hollow, while the smaller (<15 nm) nanocrystals are dense. TEM micrographs of (b,c) β-Sn nanocrystals that are predominantly rod-shaped and (d) $FeSn_2$ nanorods formed from the β-Sn nanorods in (c). SAED patterns for β-Sn nanorods and $FeSn_2$ nanorods are shown in (e) and (f), respectively.

of the β-Sn nanocrystal seeds, it is reasonable to expect that $FeSn_2$ nanocrystals with other shapes and sizes could be accessed by controlling the morphology of the β-Sn template. As a first step toward this goal, we have been able to vary the synthetic conditions to yield samples of the β-Sn nanocrystal precursors with predominantly large (>30 nm) cubes, mixtures of large (>30 nm) and small (<15 nm) cubes, and nanorods with diameters of 10−20 nm and aspect ratios of 2−4 (formed in ~60% yield), as well as large (>20 nm) and small (<10 nm) spheres. The $FeSn_2$ nanocrystals derived from predominantly large (>30 nm) cubes were shown in Figures 1 and 2, and this type of β-Sn precursor reproducibly yields hollowed-out cube-derived structures as discussed earlier. In contrast, the mixture of both large and small cube-shaped β-Sn nanocrystals generates $FeSn_2$ nanocrystals with a bimodal size distribution similar to that observed for the β-Sn seeds that are used as precursors (Figure 5a, Figure S3). In this bimodal sample, the large (~30 nm) β-Sn cubes transform to partially hollow $FeSn_2$ cube-derived nanostructures as expected. However, the small (<15 nm) β-Sn cubes transform to dense $FeSn_2$ cubes with no evidence of material depletion in the interior of the particles. (On the basis of careful SAED and EDS studies, both the small dense cubes and large etched cubes appear to be $FeSn_2$.) In both cases, the shape of the β-Sn precursors is conserved in the $FeSn_2$ product, but there is no formation of hollow structures for the smaller β-Sn cubes, implying a size-dependent reactivity regarding the hollowing-out process. Consistent with this, single-crystal β-Sn nanorods (Figure 5b,c) convert to single-crystal $FeSn_2$ nanorods (Figure 5d) with retention of the aspect ratio of the precursors. Since the nanorod diameters (e.g., the ⟨100⟩ faces) are <15 nm, no hollow structures are expected on the basis of the size-dependent observations discussed above, and none are observed.

Building on these observations of size-dependent reactivity, there also appears to be a shape-dependent reactivity associated with the Sn → $FeSn_2$ transformation. For example, β-Sn nanocrystal spheres of >20 nm diameter (Figure 6a) form $FeSn_2$ nanocrystals with predominantly dense (not hollow) cube shapes when reacted with Fe^{3+} under reducing conditions (Figure 6b). Small (<10 nm) β-Sn spheres (Figure 6c, inset) also transform into cube-shaped $FeSn_2$ nanocrystals (Figure 6c) during the chemical transformation, but with no evidence of hollow particles. Apparently, β-Sn spheres transform into $FeSn_2$ cubes, whereas β-Sn cubes retain their cube-like structure. Cubes are

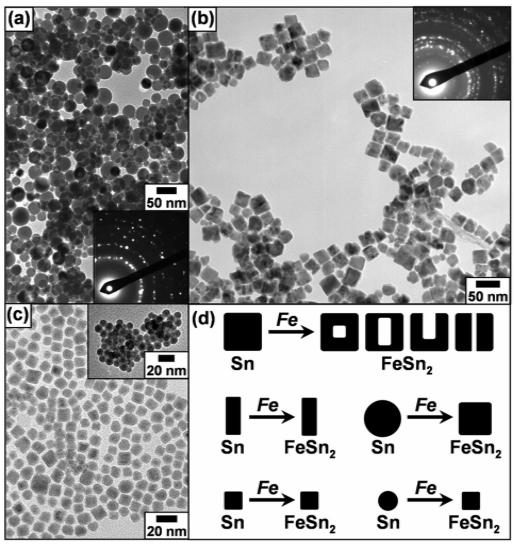

Figure 6. TEM micrographs and SAED patterns (insets) of (a) β-Sn nanospheres (mostly >20 nm), (b) $FeSn_2$ nanocubes formed from the β-Sn nanospheres in (a), and (c) $FeSn_2$ nanocubes (~10 nm) formed from the β-Sn nanospheres (<10 nm) shown in the inset. A schematic summary (qualitative, not drawn to scale) of the various β-Sn → $FeSn_2$ transformations is shown in (d).

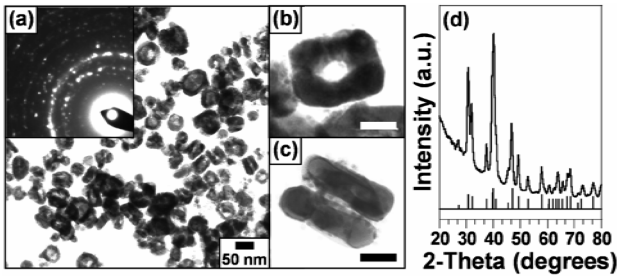

Figure 7. (a−c) TEM micrographs of cube-derived PdSn nanostructures and (d) the corresponding XRD pattern (top: experimental; bottom: pattern from PDF card #4-0803). Scale bars are 20 nm in (b) and (c).

the dominant products in both cases. However, large (>20 nm) β-Sn spheres tend to convert to dense (not hollow) $FeSn_2$ cubes, while β-Sn cubes of similar size convert to hollow or partially hollow $FeSn_2$ cubes. This means that $FeSn_2$ cubes can be generated from either spheres or cubes of β-Sn, but hollow $FeSn_2$ nanostructures can only be obtained from single-crystal β-Sn nanocube templates. The proposed pathway for the formation of hollow $FeSn_2$ cube-derived nanostructures requires single-crystal β-Sn nanocubes as precursors, and the shape-dependent reactivity we observe is consistent with this. Similar shape-dependent reactivity has been observed in a few other systems that undergo chemical transformations.[22] The $FeSn_2$ system appears to have both size- and shape-dependent reactivity, which is summarized schematically in Figure 6d.

Extension to Other Systems. This reaction strategy can also be applied to the synthesis of shape-controlled nanocrystals in other Sn-containing intermetallic systems. For example, hollow cube-derived nanocrystals of intermetallic PdSn can be formed by reacting cube-shaped β-Sn nanoparticles with Pd^{2+} under reducing conditions similar to those used to synthesize the hollow $FeSn_2$ nanostructures. Figure 7a shows a TEM image of intermetallic PdSn nanocrystals with predominantly hollow

(22) Son, D. H.; Hughes, S. M.; Yin, Y.; Alivisatos, A. P. *Science* **2004**, *306*, 1009−1012.

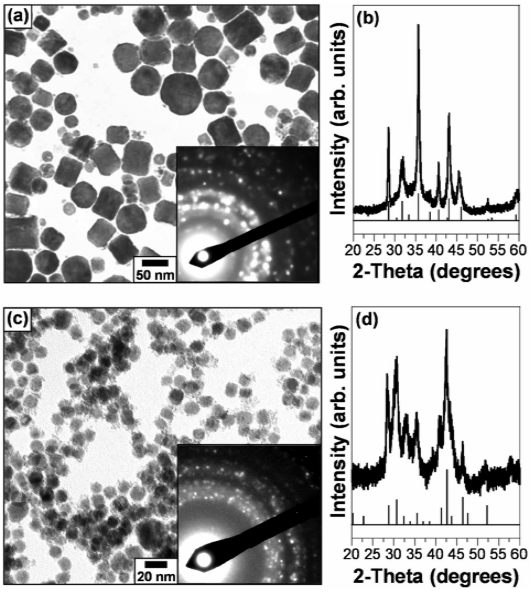

Figure 8. (a) TEM micrograph, SAED pattern (inset), and (b) XRD pattern (top: experimental; bottom: PDF card #48-1813) for α-$CoSn_3$ nanocrystals. (c) TEM micrograph, SAED pattern (inset), and (d) XRD pattern (top: experimental; bottom: modified from PDF card #37-1197 [$PtSn_3$], as described in the text) for $NiSn_3$.

square and nanorod structures (Figure 7b,c), and these are generally single-domain crystals (Figure S4), as observed for $FeSn_2$ under similar conditions. SAED (Figure 7a) and XRD (Figure 7d) data confirm the FeB-type structure of PdSn, and EDS confirms a 1:1 Pd/Sn ratio (Figure S1).

Similarly, β-Sn reacts with Co^{2+} under reducing conditions to form binary intermetallic Co−Sn nanocrystals with a mixture of spherical and cubic morphologies (Figure 8a) that matches the morphologies of the mixed cubic/spherical β-Sn precursors that were used as reactive templates (Figure S3). However, on the basis of XRD (Figure 8b), SAED (Figure 8a, inset), and EDS analysis (not shown), the Co−Sn intermetallic phase that forms is found to be α-$CoSn_3$, which is a recently discovered compound that does not appear on the originally published Co−Sn phase diagram.[14] α-$CoSn_3$ is only stable up to 275 °C, and to date, it has only been synthesized using peritectic reactions or tin flux methods.[14] When we react β-Sn nanocrystals with a stoichiometric amount of Co^{2+} under reducing conditions, α-$CoSn_3$ is reproducibly the first phase that forms in this system although, as mentioned earlier, $CoSn_2$ can also be formed when appropriate stoichiometries are used. This result shows that, in addition to forming shape-controlled intermetallic nanocrystals, this chemical conversion strategy can be used to routinely generate nanocrystals of solids that can be somewhat challenging to make using traditional solid-state synthesis methods.

Cube-shaped nanocrystals of intermetallic $NiSn_3$ can also be formed by reacting β-Sn nanocrystals with Ni^{2+} under reducing conditions in a 1:3 stiochiometric ratio (Figure 8c). Like α-$CoSn_3$, $NiSn_3$ does not appear on the published Ni−Sn phase diagram.[15] However, to our knowledge, $NiSn_3$ has not been previously reported as an isolatable solid. The XRD pattern for $NiSn_3$ (Figure 8d) matches closely with that reported for $PtSn_3$ (PDF card # 37-1197), which was reported to be a metastable high-pressure phase that also does not appear on the equilibrium Pt−Sn phase diagram.[23] $NiSn_3$ indexes to a cubic unit cell with $a = 8.75$ Å, which is contracted relative to the literature report for $PtSn_3$ ($a = 9.002$ Å),[23] as expected for the replacement of Pt with Ni. The simulated XRD pattern for $NiSn_3$, shown in Figure 8d, was generated by retaining the intensities reported for $PtSn_3$ and shifting the peaks to match those of the 8.75 Å unit cell of $NiSn_3$. The crystal structure of $PtSn_3$ has not been solved,[23] and because our $NiSn_3$ sample is nanocrystalline with very broad XRD peaks, our data are not of high enough quality to propose or refine a structure, or to eliminate the possibility of oxygen incorporation. However, the agreement between the simulated and experimental data strongly implies that the structure of $NiSn_3$ is closely related to that reported for $PtSn_3$. Importantly, this result shows that our chemical conversion strategy succeeds in stabilizing compounds that, to our knowledge, have not previously been reported using other methods. Thus, in addition to providing the ability to generate shape-controlled nanocrystals, this approach represents a potentially powerful tool for solid-state synthesis and materials discovery. Work is in progress to more fully characterize the $CoSn_3$ and $NiSn_3$ nanocrystals.

Conclusions

In this paper, we demonstrated that β-Sn nanocrystals can be used as reactive templates for the formation of intermetallic $FeSn_2$, PdSn, $CoSn_3$, and $NiSn_3$ nanocrystals via a simple solution-mediated chemical conversion strategy. This builds on other recently reported chemical conversion strategies for accessing interesting nanomaterials and represents one of only a few examples of single crystal-to-single crystal transformations in nanocrystals. The successful formation of intermetallic line compounds with narrow composition ranges highlights the degree of composition control that is achievable using this strategy and shows that ideas that are well established for intermetallic phase formation in ultrathin films and diffusion couples[24] are also applicable to the formation of bulk-scale nanocrystalline intermetallic compounds. As shown for the $FeSn_2$ system, a variety of complex cube-derived nanostructures are accessible by consideration of the size- and shape-dependent reactivity of the β-Sn precursors, as well as the anisotropic diffusion characteristics of β-Sn. For cases where β-Sn nanocrystal cubes are used as precursors, the shape is conserved in the derivative intermetallic nanocrystals, and this represents a rare single crystal-to-single crystal conversion that is likely facilitated by the similar structures of β-Sn and $FeSn_2$ (Figure S5).

While not yet exhaustive, these results provide a set of empirical guidelines for controlling the shapes of intermetallic nanocrystals that contain elements of notably different reduction potentials, reduction kinetics, and reactivity. This is especially useful because the techniques that have been developed in the past few years for perfecting the synthesis of shape-controlled metal[11] and semiconductor[25] nanocrystals do not generally appear to work well with these multimetal intermetallic systems for the reasons noted above. By combining these new guidelines for shape-controlled synthesis with our earlier studies on the synthesis and reactivity of intermetallic nanocrystals,[19,26−27] it

(23) Larchev, V.; Popova, S. *Inorg. Mater.* **1984**, *20*, 804−806.
(24) (a) Dufner, D. C. *Ultramicroscopy* **1993**, *52*, 276−281. (b) Xu, L.; Cui, Y. Y.; Hao, Y. L.; Yang, R. *Mater. Sci. Eng. A* **2006**, *435*−*436*, 638−647.
(25) Murray, C. B.; Kagan, C. R.; Bawendi, M. G. *Annu. Rev. Mater. Sci.* **2000**, *30*, 545−610.

is reasonable to anticipate that complex binary and ternary intermetallic nanocrystals in a variety of technologically useful systems may be accessible as nanoscale rods, wires, cubes, spheres, triangles, platelets, and other morphologies that are available for the elemental systems that this chemical conversion strategy utilizes as reactive templates.

In addition to its utility for generating intermetallic nanocrystals with a variety of shapes, this chemical conversion strategy has also proven to be useful for generating intermetallic compounds that can be challenging to prepare using traditional solid-state synthesis techniques. As such, it could serve as an interesting alternative to other non-equilibrium strategies for the synthesis of new, metastable, and low-temperature phases. Importantly, the temperature range in which this strategy is most successful (100−250 °C) is one that is difficult to access for intermetallics using other solid-state methods, and therefore it is reasonable to anticipate that this technique may open the door to the discovery of new compounds as nanocrystals. The ability to combine unique synthetic capabilities with shape-controlled nanocrystal synthesis using simple solution-chemistry techniques has the potential to greatly expand the complexity of solid-state materials that are accessible as nanostructures. This, in turn, will be important for accessing many technologically relevant nanomaterials, including anisotropic magnets, highly faceted nanoparticle catalysts, and nanostructures with interesting size- and dimension-dependent optical, electronic, and structural properties.

Acknowledgment. This work was supported by the National Science Foundation (DMR-0545201), the Robert A. Welch Foundation (Grant No. A-1583), the Arnold and Mabel Beckman Foundation (Young Investigator Award), and DuPont (Young Professor Grant). This material is based in part upon work supported by the Texas Advanced Research Program under Grant No. 010366-0002-2006. We thank Meg Godin for help in translating ref 23. Electron microscopy was performed at the Microscopy and Imaging Center at Texas A&M University.

Supporting Information Available: EDS element mapping for $FeSn_2$ and PdSn nanocrystals; XRD data for Sn, $CoSn_2$, and Ni_3Sn_4 nanocrystals; TEM micrographs for additional β-Sn nanocrystals; HRTEM micrograph of a PdSn nanocrystal; and a comparison of the crystal structures of β-Sn and $FeSn_2$. This material is available free of charge via the Internet at http://pubs.acs.org.

JA069032Y

(26) (a) Sra, A. K.; Schaak, R. E. *J. Am. Chem. Soc.* **2004**, *126*, 6667−6672. (b) Sra, A. K.; Ewers, T. D.; Schaak, R. E. *Chem. Mater.* **2005**, *17*, 758−766. (c) Schaak, R. E.; Sra, A. K.; Leonard, B. M.; Cable, R. E.; Bauer, J. C.; Han, Y.-F.; Means, J.; Teizer, W.; Vasquez, Y.; Funck, E. S. *J. Am. Chem. Soc.* **2005**, *127*, 3506−3515.

(27) Cable, R. E.; Schaak, R. E. *J. Am. Chem. Soc.* **2006**, *128*, 9588−9589.